JOURNAL OF GEOPHYSICAL RESEARCH, VOL. 106, NO. D17, PAGES 20,055–20,068, SEPTEMBER 16, 2001

Global observations of the carbon budget 1. Expected satellite capabilities for emission spectroscopy in the EOS and NPOESS eras

Richard J. Engelen, A. Scott Denning, Kevin R. Gurney, and Graeme L. Stephens

Department of Atmospheric Science, Colorado State University, Fort Collins, Colorado, USA

Abstract. This paper investigates the expected capabilities of the new generation of infrared satellite sounders for detecting CO_2. A general circulation model is used to simulate realistic CO_2 fields and to define the needed accuracy of CO_2 observations in order to be useful in constraining surface sources and sinks of CO_2, which will be described in more detail in a future paper. Optimal estimation retrieval theory is then used to determine the possible accuracy of the satellite measurements and to define the retrieval characteristics. A discussion of several factors that affect the retrievals is also included. We conclude that tropospheric column retrievals of CO_2 are possible with an accuracy of better than 1 ppmv on a monthly mean basis. Several factors, like thin cirrus clouds and radiative transfer modeling errors, will degrade these results if not carefully accounted for. The possibility of extensive time and spatial averaging of the satellite observations will overcome some of these problems.

1. Introduction

The development of rational policy responses to global change requires the prediction of future atmospheric CO_2 levels that result from particular anthropogenic emissions scenarios. Confident predictions of this kind require a quantitative understanding of the carbon sources and sinks in the Earth system and how they respond to land use, nutrient deposition, climate change, and CO_2 itself. Although major progress has been made in the past 10 years toward such a characterization of CO_2 sources and sinks, a quantitative accounting is not yet possible [*Houghton et al.*, 1995].

Most of what we know about the global carbon budget has been derived from the now 40-year-long record of atmospheric CO_2 sampled in clean "background" locations. These data can be interpreted with a high degree of confidence at the global scale, leading to a detailed time series of the rate of increase. The rate of combustion of fossil fuels is known from econometric tabulations [*Marland et al.*, 1989; *Andres et al.*, 1996]; so the history of atmospheric CO_2 can be used to infer the integral of all other sources and sinks in the Earth system by subtracting this anthropogenic emission rate [*Conway et al.*, 1994; *Francey et al.*, 1995; *Battle et al.*, 2000]. Such analyses have led to the conclusion that about half of the CO_2 from the emission of fossil fuels is removed from the atmosphere by sinks that vary in strength by about a factor of 2 from year to year. The cause of these interannual fluctuations is difficult to determine, as are the underlying sink mechanisms.

Paper number 2001JD900223.
0148-0227/01/2001JD900223$09.00

The nature and variability of anthropogenic carbon sinks have also been investigated using the spatial distribution of atmospheric CO_2 as measured by flask samples collected in the remote marine boundary layer. Until recently, the distribution of these flask sampling sites was so sparse that the data were only sufficient to characterize the north-south gradient. The addition of new stations and recent efforts to combine sampling networks through intercalibration [*Masarie and Tans*, 1995] have made it possible to analyze the longitudinal variations as well. Quantitative interpretation of the spatial structure of atmospheric CO_2 in terms of sources and sinks at the surface requires accounting for atmospheric transport upstream of the observing stations. This is done using numerical models in which CO_2 is transported by winds derived either from analyzed observations or from general circulation models (GCM). The process of inferring surface sources and sinks from observed concentration patterns using a transport model is referred to as "inversion" of the data [e.g., *Enting et al.*, 1995]. Inversion of the interhemispheric gradient of CO_2 concentration can be accomplished using a two-box model of atmospheric mixing; the more dense network of observing stations can only be interpreted in terms of continental fluxes with a full three-dimensional chemical tracer model (CTM).

Several groups are now using three-dimensional CTMs to perform inverse calculations of the atmospheric carbon budget with continental or regional resolution [*Fan et al.*, 1998; *Rayner et al.*, 1999; *Bousquet et al.*, 1999a, 1999b; *Kaminski et al.*, 1999; *Peylin et al.*, 2000]. Unfortunately, the current suite of carbon budget inversion studies produce results which are difficult to reconcile with one another. They agree reasonably well on the general meridional distribution (all produce sources in the tropics and sinks in the extratrop-

ics of both hemispheres) but disagree dramatically on the placement of sources and sinks at continental or ocean basin scales. *Fan et al.* [1998], for example, locate nearly all terrestrial CO_2 uptake in North America, whereas *Bousquet et al.* [1999a,1999b] estimate a stronger sink in Eurasia. *Rayner et al.* [1999] find that this sink is more evenly distributed among the northern continents.

Differences among CO_2 inversions may be due to the use of different data subsets, different mathematical treatments, or to differences in trace gas transport calculated by the suite of CTMs employed. Intercomparison experiments performed with most of these transport models find that they agree rather well at the surface in the remote marine boundary layer where concentration data are available but disagree in continental interiors and aloft where data are not available [*Law et al.*, 1996; *Denning et al.*, 1999]. Some of this disagreement among the models is due to differences in the transport by the resolved winds, but much of it has to do with parameterized vertical transport by convection and turbulence at subgrid scales. This is a particularly important problem for CO_2 transport, because convection over land is strongly correlated in time with photosynthesis, which is the dominant sink for CO_2 [*Denning et al.*, 1995, 1996].

The CO_2 inversion problem is currently data limited. Two recent studies using pseudo-data generated by models have suggested that dramatic improvements in source/sink uncertainty could be achieved by adding a few additional sampling stations over the continents [*Rayner et al.*, 1996; *Gloor et al.*, 2000]. These extra data would help constrain the carbon budgets of terrestrial ecosystems and, additionally, would reduce the freedom of the transport models to converge on the well-sampled remote marine boundary layer at the expense of strong disagreement aloft over land areas. Unfortunately, terrestrial sampling is problematic because of the heterogeneity in surface fluxes and concentrations in both space and time. *Gloor et al.* [2000] emphasized the power of frequent measurements of vertical profiles in their network optimization experiments. Airborne sampling is quite expensive, however, and difficult to deploy over some regions for logistical and political reasons.

An intriguing alternative to surface or airborne sampling is the estimation of CO_2 concentrations from data collected by space-borne sensors. This has the advantage of nearly ubiquitous coverage but is unlikely to achieve the degree of precision possible in the laboratory (typically a few tenths of a ppmv including both sampling error and analytical precision [*Masarie and Tans*, 1995]. Satellite retrievals may also have the added advantage that vertical integrals over some atmospheric columns are likely less impacted by model-to-model differences in parameterized vertical transport, which is a sensitive determinant of simulated surface concentrations [*Denning et al.*, 1999]. *Rayner and O'Brien* [2001] have evaluated the efficacy of ubiquitous column-integrated CO_2 estimates for the CO_2 inversion problem. They find that even at low precision, such data would improve retrievals of surface fluxes because of the sheer volume of the data. For monthly averaged column integrals on an 8° x 10° footprint (the resolution of their transport model), they estimate that a precision of about 2.5 ppmv or better is required to outperform the current surface observing network.

In this paper, we explore the feasibility of retrieving atmospheric CO_2 concentrations useful for inversion of surface fluxes from atmospheric infrared soundings likely to be available from space-borne instruments in the next several years. Two new infrared sounding instruments are currently being developed, the Atmospheric Infrared Sounder (AIRS) and the Infrared Atmospheric Sounding Interferometer (IASI). Both instruments will measure most of the infrared spectrum at high spectral resolution. IASI [*Diebel et al.*, 1996] is a Michelson interferometer with a spectral resolution of 0.5 cm^{-1} in the spectral range between 645 and 2760 cm^{-1} and will be launched on board of the first Meteorological Operational polar satellite (METOP) in 2003. AIRS [*Aumann and Pagano*, 1994] is an echelle spectrometer that covers the spectral range between 650 and 2700 cm^{-1} with an average resolving power of 1200 and will be launched on board of EOS-Aqua in 2001. The satellites of both instruments will fly in Sun-synchronous orbits providing two observations per day for each location on Earth (taking into account the cross-track scanning of the instruments). This work will be followed by a future paper (D. O'Brien et al., Global observations of the carbon budget, 2, CO_2 concentrations from differential absorption of reflected sunlight in the 1.61 μm band of CO_2, submitted to Journal of Geophysical Research, 2001) that explores the extent to which CO_2 concentrations can be retrieved from measurements of the absorption of reflected sunlight and the benefits of combining observations from these two measurement approaches.

We generated pseudo-data of atmospheric temperature, moisture, CO_2, and other properties using a general circulation model (GCM) and applied a radiative transfer model to calculate top-of-the-atmosphere radiances between 500 and 2500 cm^{-1} with a spectral resolution of 1 cm^{-1} consistent with the model atmosphere. We refer to these radiances as AIRS-like radiances and investigate the retrieval of CO_2 from these spectral radiances by inversion of the spectral information. Finally, we compare the resulting CO_2 estimates with the "true" values simulated by the GCM and analyze the characteristics of the error fields. In a second future paper (A.S. Denning et al., Global observations of the carbon budget, 3, Influence of space-borne data on the estimation of surface fluxes, submitted to Journal of Geophysical Research, 2001) (hereinafter referred to as Denning et al., submitted manuscript, 2001) we extend these results by investigating the use of satellite retrievals of CO_2 to estimate surface carbon sources and sinks.

The paper is organized as follows. Retrieval theory is described in section 2 followed by a description of our radiative transfer model in section 3. Section 4 describes the global circulation model we used to generate CO_2, temperature, and water vapor fields. In section 5 we present results of detailed retrieval experiments for two specific atmospheric profiles, and section 6 presents the results for global a CO_2 retrieval. Discussion of the results follows in section 7, and the paper ends with conclusions in section 8.

2. Retrieval Theory

Our retrieval of atmospheric CO_2 from high spectral resolution radiance measurements is based on optimal estimation theory as described by *Rodgers* [1976]. An observation can be described as

$$y = F(x, b) + \epsilon_y \,, \tag{1}$$

where y is the observation vector of spectral radiances; x is the vector of variables one wants to retrieve, namely atmospheric CO_2; $F(x, b)$ is the forward "real world" transfer function that links the atmospheric variables to the observations; b are all parameters that affect y but are not contained in x (such as specific absorbing gases that are specified but not retrieved, spectroscopic data, among other factors); and ϵ_y is the observational error. In our simulations the vector x contains different combinations of the atmospheric variables. In section 5.1 the vector x contains only the CO_2 profile; in section 5.2 we consider the inversion for which x contains the CO_2, temperature, and water vapor profiles; and in section 6 it contains the CO_2 profile, which is then averaged to a tropospheric mean, and the temperature and water vapor profiles. Since x can vary in the parameter sets it represents, the remainder of this section is presented in general terms and the reader can interpret x as CO_2 or a combination of CO_2, temperature, and humidity.

The real world transfer function F in (1) is approximated by some forward model (in our case a radiative transfer model)

$$y = f(x, \hat{b}) + \epsilon_f + \epsilon_y \,, \tag{2}$$

where the parameters b are estimated by $\hat{b}$ and ϵ_f is the error of the forward model. By inverting this forward model the solution vector $\hat{x}$ is obtained:

$$\hat{x} = f^{-1}(y) \,. \tag{3}$$

However, this inversion is highly unstable and amplifies the noise (ϵ_y and ϵ_f) considerably. Therefore an a priori guess profile (x_a) is used to constrain the solution. This leads us to the following representation of the retrieval scheme:

$$\hat{x} = R(y, \hat{b}, x_a) \,. \tag{4}$$

Assuming Gaussian statistics, the solution to this inverse model can be found by minimizing the following cost function with respect to $\hat{x}$:

$$\Phi = (\hat{x}-x_a)^T S_a^{-1}(\hat{x}-x_a)+[y-f(\hat{x},\hat{b})]^T S_y^{-1}[y-f(\hat{x},\hat{b})] \,. \tag{5}$$

Here S_a is the covariance matrix defining the uncertainty in x_a and S_y is the covariance matrix defining the uncertainty in y and the forward model. This is similar to a weighted least squares solution with weights S_a and S_y and also very similar in formulation to the inverse modeling problem currently used to obtain estimates of CO_2 sources and sinks from flask data [e.g., *Tarantola*, 1987; *Kasibhatla et al.*, 2000]. The solution can now be written as

$$\hat{x} = x_a + S_a K^T S_y^{-1}[y - f(\hat{x}, \hat{b})] \,. \tag{6}$$

Here $K = \partial f/\partial x$ evaluated at $\hat{x}$, which is called the weighting function matrix. Linearizing about the current estimate x_i, using $f(\hat{x}) = f(x_i) + K_i(\hat{x} - x_i) + O(\hat{x} - x_i)^2$ provides the following iterative equation to find the solution:

$$\begin{aligned} x_{i+1} = x_a + (S_a^{-1} + K_i^T S_\epsilon^{-1} K_i)^{-1} K_i^T S_\epsilon^{-1}[y \\ - f(x_i) + K_i(x_i - x_a)] \,. \end{aligned} \tag{7}$$

The covariance matrix of the solution is then

$$S_{\hat{x}} = (K^T S_\epsilon^{-1} K + S_a^{-1})^{-1} \,. \tag{8}$$

The square root of the diagonal elements of this covariance matrix represents the standard deviation of the retrieved variables and will be used as a diagnostic of the retrieval errors. The off-diagonal elements represent the correlations between the errors and are much harder to interpret.

Another useful diagnostic for the retrieval algorithm that will be used later in this paper is the averaging kernel A. Following *Rodgers* [2000], we can write the retrieved profile(s) as a linear combination of the a priori profile(s) and the real profile(s) plus an error term:

$$\hat{x} = x_a + A(x - x_a) + D_y \epsilon_y = (I - A)x_a + Ax + D_y \epsilon_y \,, \tag{9}$$

where

$$D_y = \frac{\partial R}{\partial y} = S_{\hat{x}} K^T S_\epsilon^{-1} \tag{10}$$

and

$$A = \frac{\partial \hat{x}}{\partial x} = D_y K \,. \tag{11}$$

The rows of the matrix **A** are called the averaging kernels of the retrieval and describe the sensitivity of the retrieved profile(s) to the real profile(s). They are a measure of the information content of the observations for each retrieved level and of the vertical resolution of the retrieval by means of their width and overlap, as will be shown in section 5.

3. Radiative Transfer Model and Associated Jacobians

3.1. Forward Model

The model calculates the radiation at the top of the atmosphere for a given distribution of trace gases (CO_2, H_2O, O_3, N_2O, CH_4, and O_2) and temperature. Earlier versions of the model are described by *Stephens et al.* [1996] and *Engelen and Stephens* [1997].

For the problem of relevance in this paper, the equation for the monochromatic radiance at the top of the atmosphere for a plane-parallel nonrefracted path at a certain viewing angle θ is

$$I_\nu(0, \mu) = B_\nu(T_s) e^{-\tau_s/\mu} + \int_0^{\tau_s} B_\nu(T) e^{-\tau/\mu} \mu^{-1} d\tau \,, \tag{12}$$

where

$I_\nu(\tau, \mu)$		radiance;
μ	=	$\cos\theta$;
τ		optical depth at wave number ν;
$B_\nu(T)$		Planck radiance for temperature T.

To simulate the high spectral resolution radiance data, the model uses a spectral integration at 1-cm^{-1} intervals. For a nadir sounding ($\mu = 1$), (12) becomes

$$I_i(0,1) = B_i(T_s)\,Tr(\tau_s) + \int_0^{\tau_s} B_i(T)\,Tr(\tau)d\tau\,, \quad (13)$$

where $Tr(\tau)$ is the transmittance from the top of the atmosphere to a specified level integrated over a 1-cm^{-1} spectral interval,

$$Tr(\tau) = \frac{1}{\Delta\nu}\int_{\Delta\nu} e^{-\tau_\nu} d\nu\,, \quad (14)$$

where

$$\tau_\nu = k_\nu\, u\,. \quad (15)$$

Here k_ν is the absorption coefficient and u is the amount of absorbing matter.

For the spectral band integration the Malkmus band model [*Malkmus*, 1967; *Goody and Yung*, 1989] was used. This model expresses the transmittance as a function of absorber amount at fixed pressure and temperature as

$$Tr(u) = \exp\left[-\frac{\pi\alpha_L}{2\,\delta}\left(\sqrt{1+\frac{4Su}{\pi\alpha_L}}-1\right)\right]\,, \quad (16)$$

where S is the average line intensity, α_L is the average Lorentz line width, and δ is the average line spacing. Broadband transmission is evaluated given suitable values of the band parameters α_L and S. These are obtained from line absorption data by requiring exact agreement in the weak line and strong line limits. This gives the following expression:

$$Tr(u) = \exp\left[-\frac{2X^2}{Y\Delta\nu}\left(\sqrt{1+\frac{Y^2u}{X^2}}-1\right)\right]\,, \quad (17)$$

where X and Y are related to the statistical line parameters by

$$X = \sum_i^N (S_i\,\alpha_i)^{\frac{1}{2}} \quad (18)$$

$$Y = \sum_i^N S_i \quad (19)$$

and where $\Delta\nu$ is the bandwidth. According to *Goody and Yung* [1989], the error in the band transmittance due to the use of the Lorentz line shape instead of the Voigt line shape is less than 2.6%. Because use of (18) and (19) provides band parameters that are not very accurate [*Lacis and Oinas*, 1991], the Malkmus band model parameters X and Y were calculated by least squares fitting to HITRAN96 [*Rothman et al.*, 1998] derived transmittances at a resolution of 1 cm^{-1} as a function of the optical path of the absorbers. Individual absorption lines were cut off at ± 25 cm^{-1} to comply with the absorption continuum as defined by *Clough et al.* [1989]. For water vapor the continuum is parameterized as

$$Tr(u) = \exp(-\tau_{\text{cont}})\,, \quad (20)$$

where the continuum optical depth is

$$\tau_{\text{cont}} = \nu_0\left(C_s\frac{p_w}{p_0} + C_f\frac{p}{p_0}\right)\left(\frac{T_0}{T}\right)u\,, \quad (21)$$

where u is the vertical path of water vapor; p_w and p denote the water vapor partial pressure and the ambient pressure, respectively; T is the temperature; C_s and C_f are the self- and foreign-broadening coefficients for water vapor, respectively; ν_0 is the central wave number of the band; and T_0 and p_0 are 296 K and 1013 mbar, respectively.

Because the transmission is dependent on pressure through the pressure broadening of the absorption lines and on temperature through the line strength, the Van de Hulst-Curtis-Godson (HCG) method with the temperature parameterization described by *Rodgers and Walshaw* [1966] was used to parameterize this effect. The scaled absorber amount can be written as

$$\tilde{u} = \int_{\text{path}} \Phi(T)du \quad (22)$$

and the scaled pressure is

$$\tilde{p} = \int_{\text{path}} \Psi(T)p\,du/\tilde{u}\,, \quad (23)$$

where

$$\Phi(T) = \exp[a(T-T_0) + b(T-T_0)^2] \quad (24)$$

$$\Psi(T) = \exp[a'(T-T_0) + b'(T-T_0)^2]\,. \quad (25)$$

The scaled absorber amount is applied directly in (17), and the pressure $\tilde{p}$ is used to scale the X^2 factors in (17). Defining

$$\phi = \tilde{u}\frac{\tilde{p}}{p_0}\,, \quad (26)$$

we can write the Malkmus optical depth as

$$\tau = \frac{2X^2\phi}{\Delta\nu Y\tilde{u}}\left(\sqrt{1+\frac{Y^2\tilde{u}^2}{X^2\phi}}-1\right)\,. \quad (27)$$

3.2. Jacobians

The Jacobian $\partial I/\partial q_i$, which is required for calculating the weighting function matrix, is obtained by calculating $\partial Tr_j/\partial q_i = -Tr_j\partial\tau_j/\partial q_i, j = i, N$ [*Garand et al.*, 1999], where the surface is at level N and where there is no contribution from layers above i. The Jacobian follows analytically from (27):

$$\frac{\partial\tau_j}{q_i} = \frac{2X^2}{\Delta\nu Y\tilde{u}}\left(\sqrt{1+\frac{Y^2\tilde{u}^2}{X^2\phi}}-1\right)\left(\frac{\partial\phi}{\partial q}-\frac{\phi}{\tilde{u}}\frac{\partial\tilde{u}}{\partial q}\right) + \frac{Y}{\Delta\nu\sqrt{1+\frac{Y^2\tilde{u}^2}{X^2\phi}}}\left(2\frac{\partial\tilde{u}}{\partial q}-\frac{\tilde{u}}{\phi}\frac{\partial\phi}{\partial q}\right)\,. \quad (28)$$

The Jacobian $\partial I/\partial T_i$ is obtained similarly, replacing $\partial\phi/\partial q$ and $\partial\tilde{u}/\partial q$ with $\partial\phi/\partial T$ and $\partial\tilde{u}/\partial T$, respectively. Most

quantities in (28) are stored during the forward model run, making the calculation of the Jacobians very efficient.

4. Simulated Atmospheric Data

Temperature, water vapor, and CO_2 concentration in the atmosphere and at the surface were simulated in the Colorado State University (CSU) general circulation model [e.g., *Randall et al.*, 1996; *Fowler and Randall*, 1999; *Eitzen and Randall*, 1999]. The model was integrated on a 4° x 5° (latitude by longitude) grid, with a 6-min time step. The simulated CO_2 concentration was driven by prescribed exchange at the surface.

These fluxes represent the sum of CO_2 emitted by fossil fuel combustion, air-sea gas exchange, and photosynthesis and respiration at the vegetated land surface. Fossil fuel emissions (5.8 x 10^{12} kg C yr^{-1}, or Pg C yr^{-1}) were specified according to aseasonal estimates from econometric data by *Andres et al.* [1996]. These emissions are believed to be accurate to within 10% [*Andres et al.*, 1996]. Air-sea gas exchange (with a globally integrated sink of 2.1 Pg C yr^{-1}) was specified according to estimates of *Takahashi et al.* [1999], derived by interpolation of measured sea-surface pCO_2 data and a wind speed-dependent gas exchange coefficient. These fluxes are better constrained by data in the northern Atlantic than elsewhere and are particularly uncertain in the Southern Ocean. The global integral is known to perhaps 30% [*Houghton et al.*, 1995]. Exchange with the terrestrial biosphere dominates the seasonal cycle of atmospheric CO_2 and produces very strong spatial gradients at any given time, yet has an annual magnitude smaller than the other flux components. We prescribed these exchanges according to the CASA model [*Randerson*, 1997], which uses satellite vegetation imagery and climate data to calculate photosynthesis, and a model of carbon turnover in vegetation and soils to specify respiration. The source function used here, by design, reflects a biosphere in which respiration fluxes out of the surface perfectly balance photosynthetic fluxes into the surface.

The spatial structure of the remaining CO_2 surface exchange is unknown in detail: it is the object of atmospheric inversion studies. To balance the globally averaged atmospheric carbon budget for a typical year requires a terrestrial sink in addition to the prescribed sources and sinks described above. Although recent studies agree in the magnitude of this terrestrial sink on a global scale (1.5 Pg C yr^{-1}), they use different distributions of the total flux over the continents [e.g., *Fan et al.*, 1998; *Bousquet et al.*, 1999a; *Rayner et al.*, 1999]. We prescribed this sink of 1.5 Pg C yr^{-1} as follows: 0.25 Pg C yr^{-1} of this was placed in the North American boreal region, 0.25 Pg C yr^{-1} was placed in the temperate North American region, 0.5 Pg C yr^{-1} was placed in Europe, 0.25 Pg C yr^{-1} was placed in the Asian boreal region, and 0.25 Pg C yr^{-1} was placed in temperate Asia. The removal over land was distributed spatially within each region according to the distribution of estimated net primary productivity taken from the CASA model [*Randerson*, 1997].

The GCM was then used to calculate the resulting CO_2 concentration field due to the various surface exchange processes, advection, convection, and turbulent transport. The tracer transport characteristics of the CSU GCM have been shown to produce concentration fields that are in reasonable agreement with available observations [*Law et al.*, 1996; *Denning et al.*, 1996, 1999]. Simulated values were sampled hourly and interpolated to constant pressure surfaces, then averaged to produce daily mean fields. Boundary layer values are calculated directly, since the planetary boundary layer top is a coordinate surface in the CSU GCM [*Randall et al.*, 1992]. Results were analyzed for July following a 3-year spin-up.

5. Information Content: Single-Profile Analysis

The investigation began with an extensive retrieval analysis applied to single retrieval profiles. The retrievals were performed using a 43-level tropical atmosphere. This number of levels is more than can be retrieved independently, but it allows for smoother diagnostics profiles. These diagnostics profiles can then be used to estimate the amount of independent information in the observations more accurately. For all retrievals a radiance spectrum was simulated at 1-cm^{-1} spectral resolution. Total transmittance spectra for the four most absorbing gases are shown in Figure 1. Gaussian noise was then added to these radiances to simulate the effect of instrument error (measurement noise, calibration error, etc.) on real observations. Two different CO_2 profiles were extracted from the GCM and then interpolated to the 43 pressure levels. The profiles were extrapolated into the stratosphere according to balloon observations presented by *Schmidt and Khedim* [1991]. The first profile (hereinafter referred to as NOSOURCE) is located at -62.5° longitude and 20° latitude and represents an open ocean profile with no significant CO_2 source nearby. The actual modeled CO_2 surface flux for that grid box is 0.18 μmol CO_2 m^{-2} s^{-1}. The second profile (hereinafter referred to as SOURCE) represents the American east coast and is located at -72.5° longitude and 44° latitude. The CO_2 surface flux for this grid box is 4.27 μmol CO_2 m^{-2} s^{-1}.

In the following discussion we will focus on the retrieval of CO_2 in the tropopshere, because our simulations showed that the capabilities in the stratosphere are limited. The absence of any CO_2 information in the stratosphere is explained by noting that we also have to retrieve the temperature. Information about tropospheric temperatures comes from both the CO_2 absorption bands and the almost continuous water vapor absorption band. However, stratospheric temperature information can only be retrieved from the middle of the CO_2 bands and the ozone absorption band. The total information is therefore limited and because the atmospheric temperature signal is stronger than the CO_2 signal, the temperature retrieval is favored above the CO_2 retrieval.

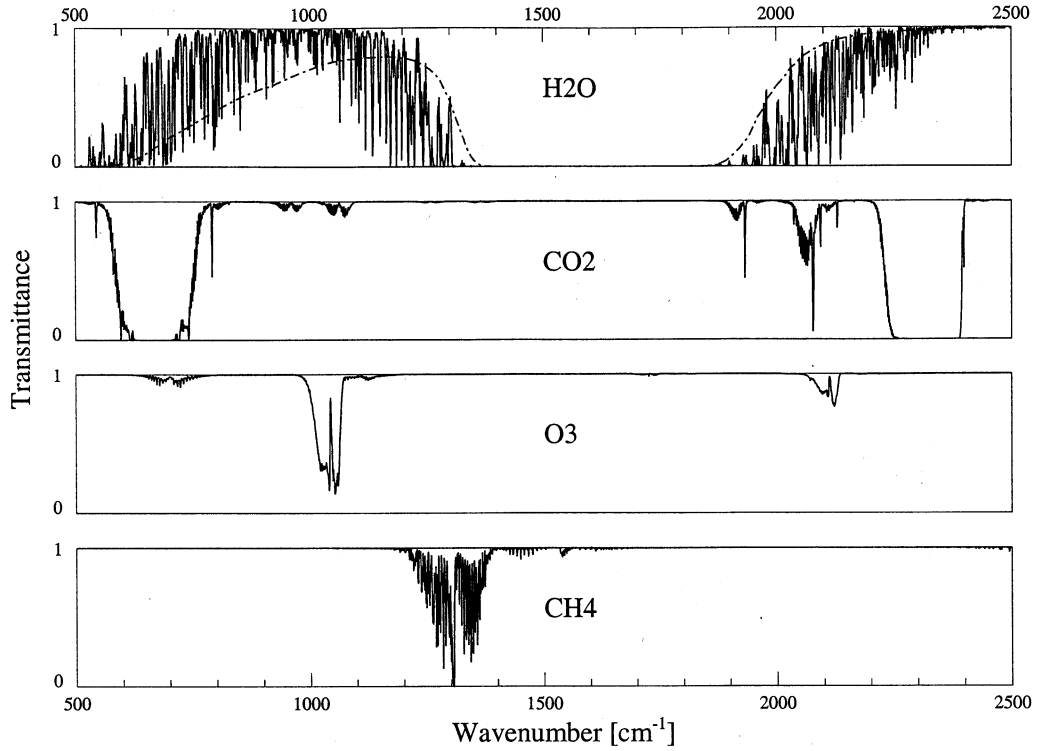

Figure 1. Total transmittance spectra between 500 cm^{-1} and 2500 cm^{-1} for water vapor (continuum represented by dashed line), carbon dioxide, ozone, and methane.

5.1. CO_2 Only

The first retrieval experiment conducted is for a CO_2 retrieval only. The profiles of all other gases as well as the temperature profile are assumed known. The measurement error of the radiances used to specify the measurement covariance matrix is 0.5%, which corresponds roughly to a 0.3 K error in brightness temperatures consistent with or even higher than measurement errors associated with AIRS or IASI. The a priori CO_2 error is assumed to be 4 ppmv, which is approximately equal to the pole-pole gradient in annual mean CO_2 and therefore a measure of the uncertainty in the CO_2 fields produced by the GCM. The a priori CO_2 profile is taken to be well mixed with a value of 370 ppmv in the troposphere and 360 ppmv in the stratosphere with a linear interpolation between the two regimes. Figure 2a shows the model-derived CO_2 profile (solid line), the a priori profile (dashed line), and the retrieved profile (thick line) for the NOSOURCE profile.

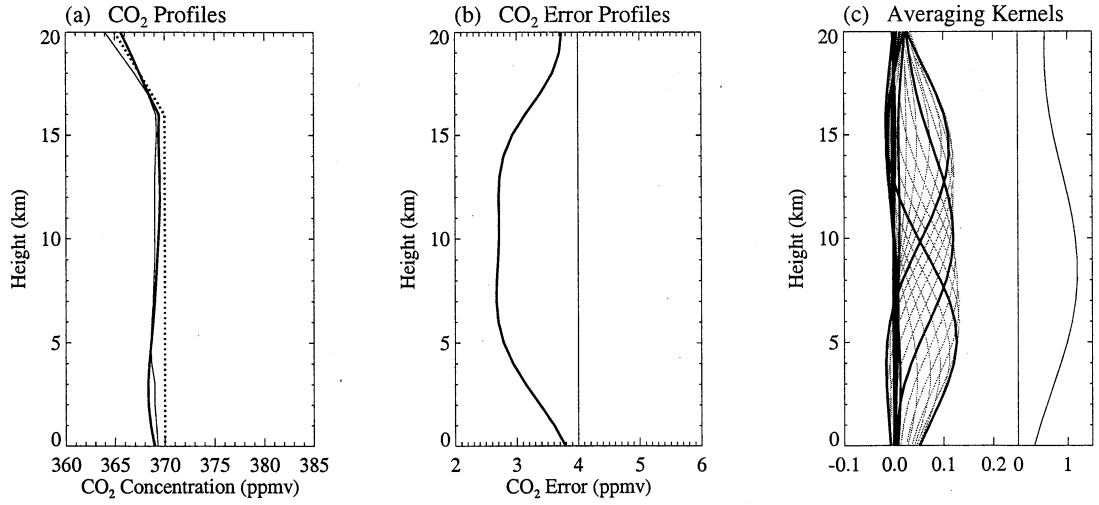

Figure 2. Retrieval results for a CO_2-only retrieval for the NOSOURCE profile (see text). Gaussian noise is added to the simulated observations. (a) A priori (dotted line), real (thin line), and retrieved (thick line) profiles; (b) a priori (thin line) and retrieval (thick line) errors; (c) averaging kernels (see text for explanation).

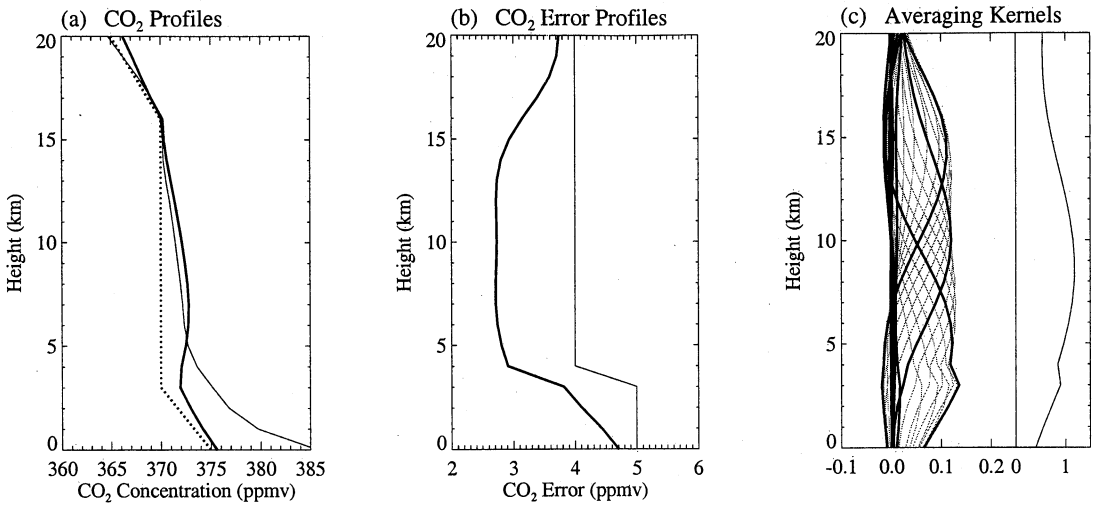

Figure 3. Same as Figure 2, but for the SOURCE profile.

The retrieval seems to do reasonably well in the troposphere. This is further illustrated by Figure 2b, in which the estimated retrieval error is shown (the diagonal elements of the matrix $S_{\hat{x}}$, which are used in the GCM inversion as an estimate of the retrieval errors). The initial a priori error of 4 ppmv is most reduced in the troposphere between about 5 and 15 km. Figure 2c shows the rows of the A matrix (averaging kernels) with every fifth row shown as a thick line for clarity. The curve to the right is produced by calculating for each retrieved level the area of the respective averaging kernel curve. The value of the quantity plotted in this panel should approach unity for a retrieval independent of the a priori constraint [e.g., *Engelen and Stephens*, 1999]. The averaging kernels are also good indicators of the vertical resolution of the retrieval. It is clear that the kernels are very broad and overlap considerably, suggesting a significant degree of correlation between layers. Figure 2c also shows that the sensitivity is largest in the middle and upper troposphere and that the sensitivity in the boundary layer is almost negligible. Lack of sensitivity in the boundary layer is unfortunately a characteristic weakness of the emission-based observing system, especially given the desire to detect changes in boundary layer where the spatial structure due to the various CO_2 sources and sinks is strongest.

The lack of sensitivity in the boundary layer is even better illustrated in Figure 3, which presents the same retrieval diagnostics, but now for the SOURCE profile. The a priori profile was changed to account for some knowledge about CO_2 profiles over industrialized regions by increasing mixing ratios below 3 km. The a priori error profile is changed to 5 ppmv below 3 km to acknowledge the increased uncertainty in boundary layer values. The estimated retrieval error (Figure 3b) and the averaging kernels (Figure 3c) are changed in the lower troposphere compared with Figure 2, because the a priori error profile changed. Most pronounced, however, is the retrieval problem in the boundary layer as illustrated with Figure 3a. The retrieved profile is clearly drawn to the a priori profile in the lowest part of the troposphere owing to the minimal information content in the observations. In the middle and upper troposphere the retrieval performs rather well, getting close to the real profile well within the error margin.

For the results in Figure 4, we removed the noise from the simulated measurements and brought the error estimates in S_y down from 0.5% to 0.1%. The figure shows that the retrieved profile is much improved with smaller error throughout. The averaging kernels are narrower, and their areas are closer to the desired value of unity. However, difficulties remain for the boundary layer retrieval where the inversion relies on the a priori information because of the lack of sensitivity of the observations to changes in boundary layer CO_2. As mentioned above, this low sensitivity is characteristic for emission-based sounding methods and occurs because of the lack of temperature contrast between the surface and the boundary layer. Consequently, the quality of boundary layer retrievals is less than desired and varies with different meteorological situations. The assumption of no measurement noise in this last experiment is of course unrealistic and serves only as a comparison for the other retrievals.

5.2. CO_2, Temperature, and Water Vapor

In this retrieval experiment we assume we have some a priori knowledge about the temperature and water vapor profiles, but unlike the previous section this knowledge is not precise. Therefore we add the profiles of temperature and water vapor to the retrieval vector and retrieve temperature, water vapor, and CO_2 simultaneously. The a priori temperature and water vapor profiles were taken from the model profiles by shifting these profiles 1 K and 10%, respectively. The a priori error estimates for temperature are taken to be 1 K and for water vapor 10%, which is consistent with the background error standard deviation used in the European Centre for Medium-Range Weather Forecasts (ECMWF) data assimilation [e.g., *Prunet et al.*, 1998; *Derber and Bouttier*, 1999; *Fillion and Mahfouf*, 2000].

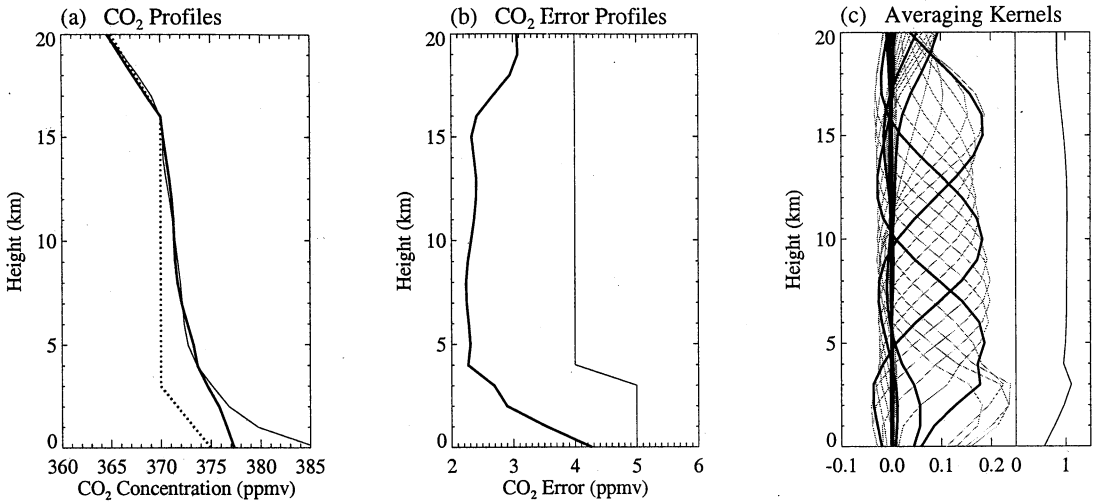

Figure 4. Same as Figure 2, but for the SOURCE profile and with noise-free observations.

The CO_2 a priori is the same as in the first experiment. Both the temperature and water vapor error covariances have off-diagonal elements (representing correlations between the layers), and we introduce this correlation in the form

$$S_a(i,j) = \sqrt{S_a(i,i)S_a(j,j)}\exp\{-[z(i) - z(j)]^2/L^2\}, \quad (29)$$

where S_a is the respective error covariance matrix, z is the level height, and L is the correlation length scale.

Figure 5 shows the retrieval results for the same NOSOURCE CO_2 profile as in the earlier experiments. The differences between the CO_2-only retrieval and this full retrieval are rather small. The averaging kernels (Figure 5c) are somewhat broader and have a smaller amplitude than that in the CO_2-only case. The retrieval error profile (Figure 5b) has increased slightly. Finally, the retrieved profile in Figure 5a closely approaches the real profile in the free troposphere but remains fixed to the a priori value above 15 km.

The error statistics for the SOURCE profile, shown in Figure 6, are similar to the NOSOURCE case. However, the problem with the almost nonexistent vertical resolution, as depicted by the averaging kernel functions, shows now in the retrieved profile. Forced by the well-mixed a priori profile with increased mixing ratios in the lower troposphere, it underestimates the real profile in the lower troposphere and overestimates the real profile in the upper troposphere. The latter effect is due to the fact that the a priori mixing ratios in the stratosphere are higher than the real mixing ratios (not shown). The retrieved profile stays, however, within the estimated error from the real profile at all levels.

To illustrate the effect of measurement noise on the retrieval, Figure 7 shows the full retrieval without Gaussian noise added to the simulated measurements. It is clear

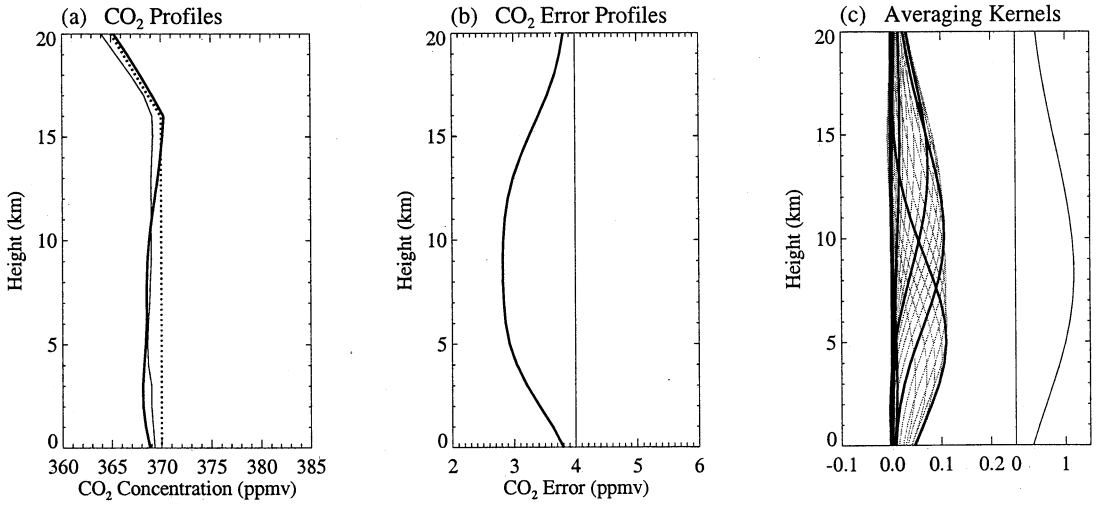

Figure 5. CO_2 retrieval results for a full retrieval for the NOSOURCE profile. Gaussian noise is added to the simulated observations. (a) A priori (dotted line), real (thin line), and retrieved (thick line) profiles; (b) a priori (thin line) and retrieval (thick line) errors; (c) averaging kernels (see text for explanation).

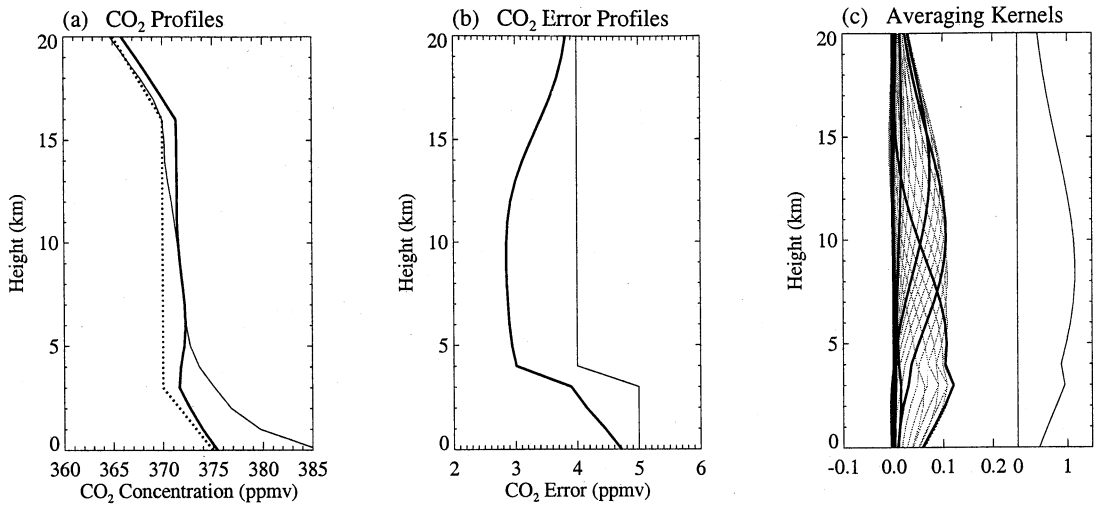

Figure 6. Same as Figure 5, but for the SOURCE profile.

that there is much better vertical resolution and that there is also some information in the stratosphere. The error profile shows a larger error reduction than the two cases with measurement noise. The retrieved profile is also much closer to the real profile.

We conclude from these single profile retrievals that it may be possible to retrieve vertical variations of CO_2 in the free troposphere with an accuracy approaching 2.5-3 ppmv. Retrieving an integrated tropospheric quantity will reduce these errors even more, as will be shown in the next section. The magnitude of these retrieval errors are shown in a related paper (Denning et al., submitted manuscript, 2001] and by *Rayner and O'Brien* [2001] to have significant positive influence on CO_2 inversions. However, the uncertainty in the temperature and water vapor profiles prohibits any retrieval in the stratosphere, and the lack of contrast between the surface and the boundary layer temperature together with the lack of significant temperature gradient in the boundary layer prohibits any meaningful retrieval in the boundary layer. Using temperature and water vapor retrievals from other instruments on board of the same platform (e.g., the Advanced Microwave Sounding Unit and the Humidity Sounder for Brazil) will help considerably to improve retrieval accuracy and to retrieve stratospheric CO_2 as well.

6. Global Retrievals

Daily mean simulated fields of temperature, water vapor, and CO_2 for July from the CSU GCM were used to perform a global retrieval experiment. For every grid box the radiance at the top of the atmosphere was calculated between 500 and 2500 cm^{-1} at 1-cm^{-1} spectral resolution. Gaussian noise with a standard deviation of 0.5% was then added to these calculated radiances to simulate the satellite observations.

Because the analyses in section 5 showed that most CO_2 information is in the troposphere without any significant ver-

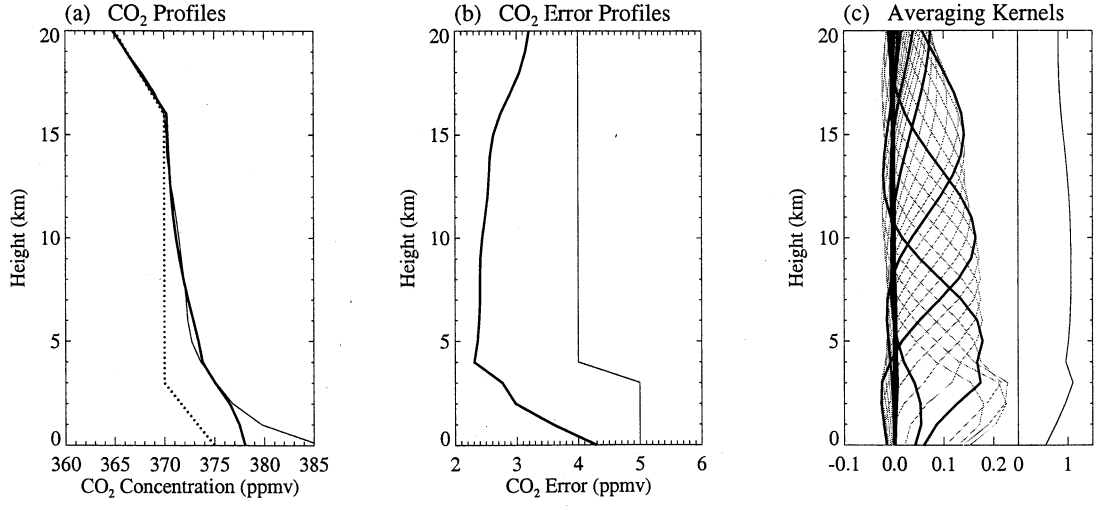

Figure 7. Same as Figure 5, but for the SOURCE profile with noise-free observations.

tical resolution, the global retrieval described in this section was set up to retrieve a CO_2 profile that was then averaged to provide a column amount. The weighting for the averaging was defined by the total averaging kernel profiles (see, for example, Figure 6c). These same weighting profiles were also applied to the modeled CO_2 fields to provide fields that are then directly comparable to the retrieved CO_2 fields.

The a priori fields were constructed as above by shifting the temperature profiles by 1 K and the water vapor profiles by 10%. For each retrieved profile, these shifts were randomly defined as a positive or negative shift. The a priori CO_2 value was set to a monthly averaged zonal mean constant value throughout the atmosphere. The meridional gradients are expected to be available from flask data, and the strength of the satellite retrieval is as a correction for longitudinal structure. The a priori covariance matrix was constructed with a 1 K standard deviation for the temperature profile, a 10% standard deviation for the water vapor profile, and a 4 ppmv standard deviation for CO_2. Correlation between layers for both temperature and water vapor was specified according to (29). No correlation between temperature and water vapor was used. Clouds were introduced by using a total cloud mask for each day based on a typical July month from the ECMWF reanalysis [*Gibson et al.*, 1999]. If a grid box was more than 80% cloudy, no retrieval was performed.

Plate 1 shows the simulated CO_2 retrieval results. The retrieved CO_2 field and the a priori guess are shown in Plates 1a and 1b, respectively. The weighted model CO_2 values and the difference between these and the retrieved values are shown in Plates 1c and 1d. The figures show that the retrieval is able to adjust the a priori guess considerably to provide the spatial pattern that is present in the modeled CO_2 field. The difference map in Plate 1d shows only small differences over the entire globe. This is also illustrated by Figure 8a, in which a histogram of these differences is plotted. On a monthly mean basis the root-mean-square (RMS) differences are 0.47 ppmv with a global mean error of -0.16 ppmv. It is important, however, to realize that these retrieval results are weighted averages of the tropospheric CO_2 mixing ratios. Plate 1e shows the unweighted tropospheric mean CO_2 distribution from the model. The general pattern is the same as in Plate 1c, but the absolute values differ. This is entirely due to the inability to retrieve CO_2 values in the lowermost atmosphere. The difference plot between the retrieved values and the unweighted model values in Plate 1f also illustrates this. Although the differences are generally still within 1 ppmv as shown in Figure 8b, there are now areas with larger deviations. The RMS error is now 0.97 ppmv and the global mean error is -0.52 ppmv. The differences are largest in areas where strong sinks act to reduce the boundary layer CO_2 concentrations. It is therefore important to account for the weighting when using the retrieved CO_2 values in a model inversion. This last argument is exactly the reason why, for instance, numerical weather forecast models tend to assimilate radiances instead of atmospheric variables. The weighting inherent to remotely sensed observations is then implicitly carried out inside the data assimilation model.

7. Discussion

The above sections described the potential of high spectral resolution infrared satellite observations to retrieve atmospheric CO_2 concentrations. Although the results look promising, there are some caveats that have to be noted:

1. We simulated a spectrum between 500 cm^{-1} and 2500 cm^{-1} with a spectral resolution of 1 cm^{-1}. The observations of instruments like AIRS and IASI will have different spectral ranges and spectral resolutions. For instance, AIRS will have a spectral resolution of $\lambda/\Delta\lambda = 1200$, which is slightly better than the assumed 1 cm^{-1} at smaller wavelengths (higher wave numbers) and slightly worse at longer wavelengths (smaller wave numbers). A detailed assessment of the performance of any given instrument requires the use of exact wave number characteristics of the specific instrument in question.

2. We used a reasonable measurement error in our analyses but neglected any errors in the radiative transfer modeling. Modeling errors with a Gaussian character will increase our final retrieval errors. However, the main problem with radiative transfer errors lies in unknown biases. Because of the small variations in CO_2 we are trying to detect, small

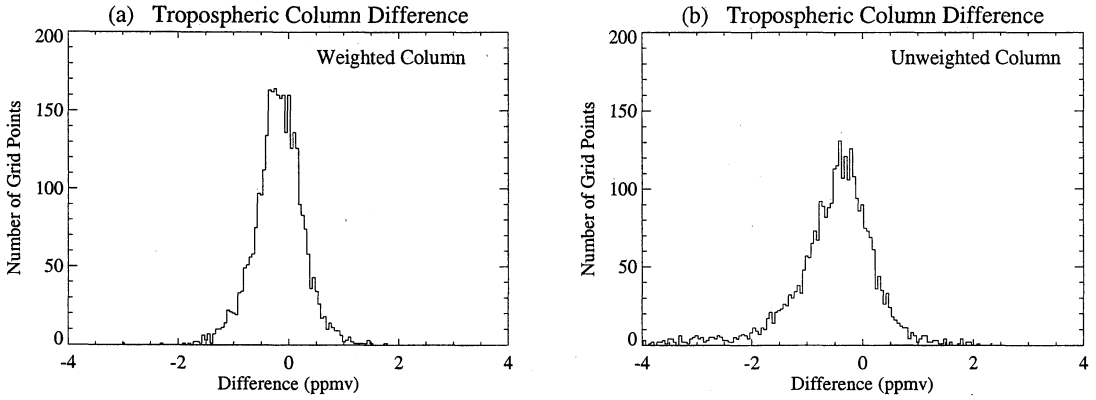

Figure 8. Histogram of (a) retrieved CO_2 values minus weighted model CO_2 values and (b) of retrieved CO_2 values minus unweighted model CO_2 values.

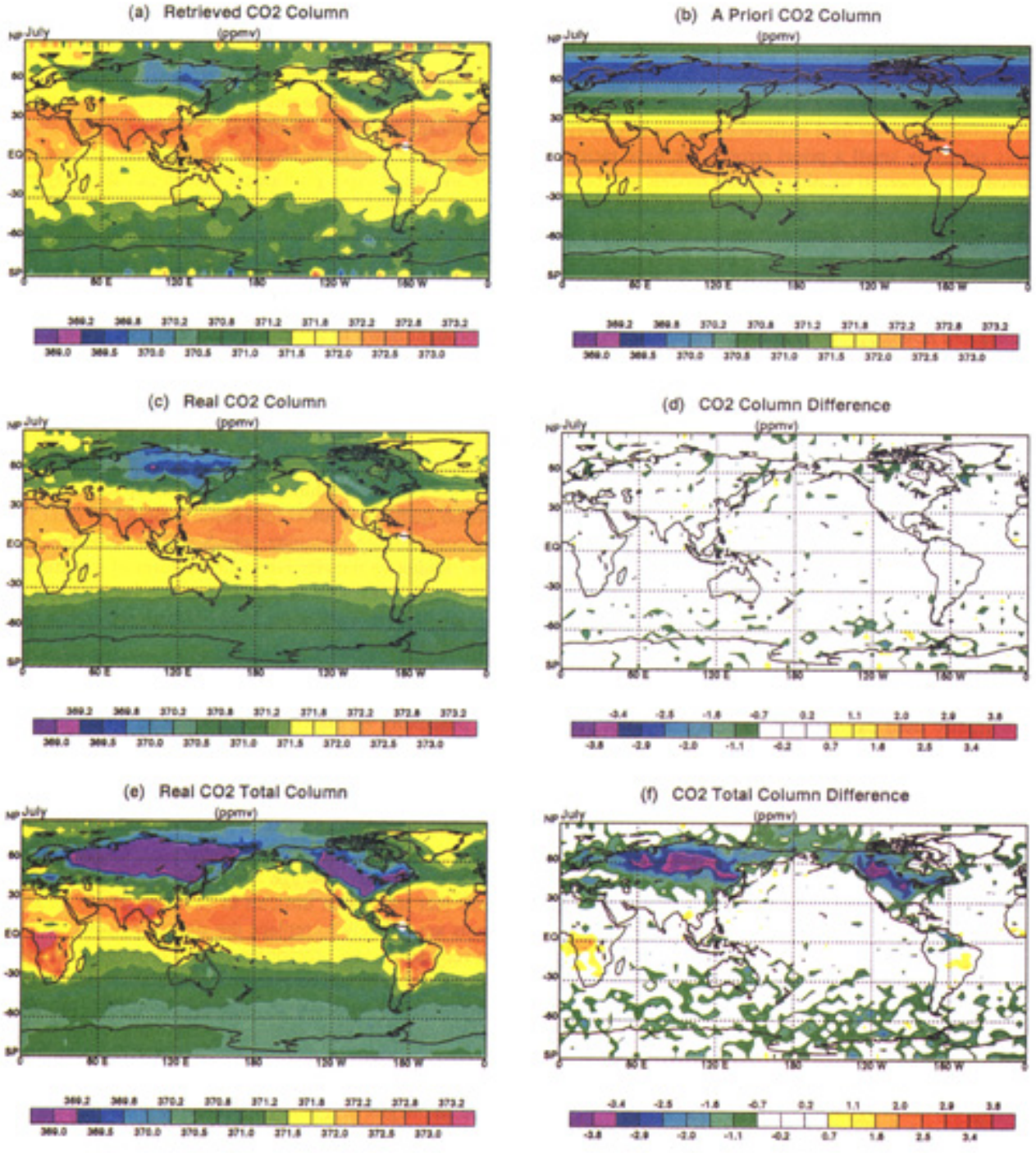

Plate 1. Monthly mean tropospheric averaged CO_2 results for a full global retrieval with (a) the retrieved values, (b) the a priori values, (c) the real CO_2 values weighted by the retrieval averaging kernels, (d) the difference between Plate 1c and Plate 1a, (e) the unweighted real values, and (f) the difference between Plate 1e and Plate 1a.

errors arising from uncertainties in, for instance, the spectroscopy could render retrievals useless. Thus it remains an important task to define and monitor the nature of possible bias errors. Matching satellite radiances to current surface measurement networks is thus essential for this purpose. Given the middle tropospheric weighting of the satellite retrievals, in situ measurements by airborne sampling will also be crucial.

3. Uncertainties in the a priori temperature and water vapor profiles affect the final retrieval errors. In this study, we apply relatively small a priori errors. We have tacitly assumed that numerical weather forecast models will be accurate enough, especially if combined with temperature and water vapor retrievals from microwave instruments. This may be a reasonable assumption given that current model uncertainties used in the data assimilation at ECMWF are similar to those assumed in this study [e.g., *Prunet et al.*, 1998; *Derber and Bouttier*, 1999; *Fillion and Mahfouf*, 2000].

4. The presence of clouds affects the retrievals. Undetected clouds like thin cirrus will bias the retrievals through their effect on the radiances. Thick clouds in the middle and upper troposphere will prohibit a retrieval. Fortunately, the time sampling needed for worthwhile CO_2 inversions is not a restricting factor. Inversion modeling is typically applied to produce monthly mean CO_2 source and sink data, and any measurement that is available on a daily or almost daily basis has significant value. Of course, geographical areas with persistent cloud cover will be largely undersampled, and these could cause some problems in the inverse CO_2 modeling. It is also important to realize that the footprint of an instrument like AIRS is of the order of 20 km, which allows many samples within a coarse GCM grid box as currently used in inversion studies. Therefore partial cloud cover within a grid box will still allow enough CO_2 retrievals to be useful in the inverse modeling process, and spatial averaging of many 20-km retrievals within a grid box will substantially reduce errors.

5. A further sampling problem is the time sampling typical of polar orbiters. Observations are only available twice a day for a single satellite at the same local time every day. If there exists a significant diurnal cycle in the CO_2 field, this could be a further source of bias. However, this sampling effect is likely to be most significant in the boundary layer and therefore less of a problem for emission-based observations with a middle tropospheric weighting.

8. Conclusions

Inverse modeling of CO_2 is currently used to infer estimates of sinks and sources of atmospheric CO_2 from observations. Sampling of the current network of surface observations, however, is limited in both time and space and severely restricts our ability to detect the global distribution of CO_2 sources and sinks. This paper is part of a series that attempts to examine how satellite measurements might alleviate this problem. The present paper examines the potential of new generation infrared sounders for retrieving CO_2.

The new generation infrared satellite sounders will provide measurements over the whole infrared region of the spectrum at high spectral resolution. The sampling of these observing systems provides observations at much higher time and space resolution and may therefore add considerable information to the inverse modeling problem if the CO_2 observations from these instruments are accurate enough [*Rayner and O'Brien*, 2001; Denning et al., submitted manuscript, 2001].

Several retrieval experiments were performed to illustrate the potential of these satellite observations for the detection of atmospheric CO_2. Retrieval of single profiles showed that the information per level is limited, even if the temperature and water vapor profiles are known exactly. CO_2 information is mainly restricted to the free troposphere with no information in the boundary layer and little information in the stratosphere. Global CO_2 retrievals for each day in July were carried out to provide a monthly mean weighted tropospheric CO_2 amount. Results show that retrieval errors can be brought down to about 1 ppmv. Retrievals of this quality are useful in the inverse modeling as will be shown in a future paper (Denning et al., submitted manuscript, 2001).

Finally, several pros and cons were described that will affect these retrievals. Clouds will degrade the retrievals, but the excellent sampling of the satellite systems combined with the coarser resolution requirements of source/sink inversion studies will allow for careful sampling of clear skies and considerable averaging, which will bring down the errors. Radiative transfer errors in the form of spectroscopy errors remain a source of concern, mainly because these errors are likely to enter in the form of biases rather than in the form of random noise.

In view of the spatial noise in the retrieved CO_2 field, the difficulty of obtaining near-surface concentrations, and the possibility of biased retrievals due to errors in radiative transfer models, we stress the need for continued surface measurements and new in situ airborne measurements in the free troposphere in combination with any future satellite observations. The value of the space-based data for the CO_2 inverse problem lies in the huge increase in both spatial and temporal coverage and the ability to sample many areas that have been difficult to sample. These measurements are unlikely to replace the surface network. Rather, the very dense, low-precision sampling possible from spaceborne sensors should be seen as a potentially valuable complement to the very sparse, high-precision flask programs. Because of their high accuracy, observations from the current surface network will remain vital to detect possible biases in the satellite observations and thus must be considered to be an integral part of any space-based observing system.

We conclude that CO_2 information extracted from AIRS and IASI sounders has considerable promise and can fill an existing gap in global observations until more capable observing systems, such as those based on the lidar method, are developed.

Acknowledgments. The work described in this paper was supported by DOC-NOAA contract NA67RJ0152 Amend 25, by a NASA Carbon Cycle Science grant for the project 'Global and Regional Carbon Flux Estimation using Atmospheric CO_2 Measurements from Spaceborne and Airborne Instruments', and by NSF grant ATM-9711616.

References

Andres, R., G. Marland, I. Fung, and E. Matthews, A 1 x 1 distribution of carbon dioxide emissions from fossil fuel consumption and cement manufacture, 1950-1990, *Global Biochem. Cycles*, *10*, 419–430, 1996.

Aumann, H., and R. Pagano, The atmospheric infrared sounder on EOS, *Opt. Eng.*, *32*, 776–784, 1994.

Battle, M., M. Bender, P. Tans, J. White, J. Ellis, T. Conway, and R. Francey, Global carbon sinks and their variability inferred from atmospheric O_2 and 13C, *Science*, *287*, 2467–2470, 2000.

Bousquet, P., P. Ciais, P. Peylin, M. Ramonet, and P. Monfray, Inverse modeling of annual atmospheric CO_2 sources and sinks, 1, Method and control inversion, *J. Geophys. Res.*, *104*, 26,161–26,178, 1999a.

Bousquet, P., P. Ciais, P. Peylin, M. Ramonet, and P. Monfray, Inverse modeling of annual atmospheric CO_2 sources and sinks, 2, Sensitivity study, *J. Geophys. Res.*, *104*, 26,179–26,194, 1999b.

Clough, S., F. Kneizys, and R. Davies, Line shape and the water vapor continuum, *Atmos. Res.*, *23*, 229–241, 1989.

Conway, T., P. Tans, L. Waterman, K. Thoning, D. Kitzis, K. Masarie, and N. Zhang, Evidence for interannual variability of the carbon cycle from the NOAA/CMDL global air sampling network, *J. Geophys. Res.*, *99*, 22,831–22,855, 1994.

Denning, A., I. Fung, and D. Randall, Latitudinal gradient of atmospheric CO_2 due to seasonal exchange with land biota, *Nature*, *376*, 240–243, 1995.

Denning, A., D. Randall, G. Collatz, and P. Sellers, Simulations of terrestrial carbon metabolism and atmospheric CO_2 in a general circulation model, 2, Spatial and temporal variations of atmospheric CO_2, *Tellus, Ser. B*, *48*, 543–567, 1996.

Denning, A., et al., Three-dimensional transport and concentration of SF6: A model intercomparison study (TransCom 2), *Tellus, Ser. B*, *51*, 266–297, 1999.

Derber, J., and F. Bouttier, A reformulation of the background error covariance in the ECMWF global data assimilation system, *Tellus, Ser. A*, *51*, 195–221, 1999.

Diebel, D., F. Cayla, and T. Phulpin, Mission rationale and requirements, *Tech. Rep. IA-SM-0000-10-CNE/EUM*, issue 3, CNES/EUMETSAT, Cent. Natl. d'Etudes Spatiales, Toulouse, France, 1996.

Eitzen, Z., and D. A. Randall, Sensitivity of the simulated Asian summer monsoon to parameterized physical processes, *J. Geophys. Res.*, *104*, 12,177–12,191, 1999.

Engelen, R. J., and G. L. Stephens, Infrared radiative transfer in the 9.6-μm band: Application to TOVS ozone retrieval, *J. Geophys. Res.*, *102*, 6929–6940, 1997.

Engelen, R. J., and G. L. Stephens, Characterization of water vapour retrievals from infrared TOVS radiances and microwave SSM/T-2 radiances, *Q. J. R. Meteorol. Soc.*, *125*, 331–351, 1999.

Enting, I., C. Trudinger, and R. Francey, A synthesis inversion of the concentration and d13C of atmospheric CO_2, *Tellus, Ser. B*, *47*, 35–52, 1995.

Fan, S.-M., M. Gloor, J. Mahlman, S. Pacala, J. Sarmiento, T. Takahashi, and P. Tans, A large terrestrial carbon sink in North America implied by atmospheric data and oceanic carbon dioxide data and models, *Science*, *282*, 442–446, 1998.

Fillion, L., and J.-F. Mahfouf, Coupling of moist-convective and stratiform precipitation processes for variational data assimilation, *Mon. Weather Rev.*, *128*, 109–124, 2000.

Fowler, L., and D. Randall, Simulation of upper tropospheric clouds with the CSU general circulation model, *J. Geophys. Res.*, *104*, 6101–6121, 1999.

Francey, R., P. Tans, C. Allison, I. Enting, J. White, and M. Trolier, Changes in the oceanic and terrestrial carbon uptake since 1982, *Nature*, *373*, 326–330, 1995.

Garand, L., D. Turner, C. Chouinard, and J. Hallé, A physical formulation of atmospheric transmittances for the massive assimilation of satellite infrared radiances, *J. Appl. Meteorol.*, *38*, 541–554, 1999.

Gibson, J., P. Kållberg, S. Uppala, A. Hernandez, A. Nomura, and E.Serrano, ERA description, *ECMWF Re-Analysis Proj. Rep. Ser.* 1, Eur. Cent. for Medium-Range Weather Forecasts, Reading, England, UK, 1999.

Gloor, M., S.-M. Fan, S. Pacala, and J. Sarmiento, Optimal sampling of the atmosphere for purpose of inverse modeling: A model study, *Global Biogeochem. Cycles*, *14*, 407–428, 2000.

Goody, R., and Y. Yung, *Atmospheric Radiation: Theoretical Basis*, 2nd ed., Oxford Univ. Press, New York, 1989.

Houghton, J., L. Filho, B. Callandar, N. Harris, A. Kattenberg, and K. Maskell, *Climate Change 1995: Contribution of Working Group 1 to the Second Assessment Report of the Intergovernmental Panel on Climate Change*, Cambridge Univ. Press, New York, 1995.

Kaminski, T., M. Heimann, and R. Giering, A coarse grid three-dimensional global inverse model of the atmospheric transport, 2, Inversion of the transport of CO_2 in the 1980s, *J. Geophys. Res.*, *104*, 18,555–18,581, 1999.

Kasibhatla, P., M. Heimann, P. Rayner, N. Mahowald, R. Prinn, and D. Hartley, eds., *Inverse Methods in Global Biogeochemical Cycles*, Geophys. Monogr. Ser., vol. 114, AGU, Washington, D. C., 2000.

Lacis, A., and V. Oinas, A description of the correlated k distribution method for modeling nongray gaseous absorption, thermal emission, and multiple scattering in vertically inhomogeneous atmospheres, *J. Geophys. Res.*, *96*, 9027–9063, 1991.

Law, R., et al., Variations in modeled atmospheric transport of carbon dioxide and the consequences for CO_2 inversions, *Global Biogeochem. Cycles*, *10*, 783–796, 1996.

Malkmus, W., Random Lorentz band model with exponential-tailed s^{-1} line-intensity distribution function, *J. Opt. Soc. Am.*, *575*, 323–329, 1967.

Marland, G., T. Boden, R. Griffith, S. Huang, P. Kanciruk, and T. Nelson, Estimates of CO_2 emissions from fossil fuel burning and cement manufacturing, based on the U.S. Bureau of Mines cement manufacturing data, technical report, Carbon Dioxide Inf. Anal. Cent., Oak Ridge, TN, 1989.

Masarie, K., and P. Tans, Extension and integration of atmospheric carbon dioxide data into a globally consistent measurement record, *J. Geophys. Res.*, *100*, 11,593–11,610, 1995.

Peylin, P., P. Bousquet, P. Ciais, and P. Monfray, Differences in CO_2 flux estimates based on a time-independent versus a time-dependent inversion method, in *Inverse Methods in Global Biogeochemical Cycles, Geophys. Monogr. Ser.*, vol. 114, edited by P. Kasibhatla et al., pp. 811–841, AGU, Washington, D. C., 2000.

Prunet, P., J.-N. Thépaut, and V. Cassé, The information content of clear sky IASI radiances and their potential for numerical weather prediction, *Q. J. R. Meteorol. Soc.*, *124*, 211–241, 1998.

Randall, D., Q. Shao, and C.-H. Moeng, A second-order bulk boundary-layer model, *J. Atmos. Sci.*, *49*, 1903–1923, 1992.

Randall, D., et al., A revised land-surface parameterization (SiB2) for atmospheric GCMs, part 3, The greening of the CSU general circulation model, *J. Clim.*, *9*, 738–763, 1996.

Randerson, J., The contribution of terrestrial sources and sinks to trends in the seasonal cycle of atmospheric carbon dioxide, *Global Biogeochem. Cycles*, *11*, 535–560, 1997.

Rayner, P., and D. O'Brien, The utility of remotely sensed CO_2 concentration data in surface source inversions, *Geophys. Res. Lett.*, *28*, 175–178, 2001.

Rayner, P., I. Enting, and C. Trudinger, Optimizing the CO_2 observing network for constraining sources and sinks, *Tellus, Ser. B*, *48*, 433–444, 1996.

Rayner, P., I. Enting, R. Francey, and R. Langenfelds, Reconstructing the recent carbon cycle from atmospheric CO_2, d13C, and O_2/N_2 observations, *Tellus, Ser. B*, *51*, 213–232, 1999.

Rodgers, C., Retrieval of atmospheric temperature and composition from remote measurements of thermal radiation, *Rev. Geophys.*, *14*, 609–624, 1976.

Rodgers, C., *Inverse Methods for Atmospheric Sounding. Theory and Practice*, World Sci., River Edge, N. J., 2000.

Rodgers, C., and C. Walshaw, The computation of infrared cooling rate in planetary atmospheres, *Q. J. R. Meteorol. Soc.*, *92*, 67–92, 1966.

Rothman, L., et al., The HITRAN molecular spectroscopic database and HAWKS (HITRAN Atmospheric Workstation): 1996 edition, *J. Quant. Spectrosc. Radiat. Transfer*, *60*, 665–710, 1998.

Schmidt, U., and A. Khedim, In situ measurements of carbon dioxide in the winter Artic vortex and at midlatitudes: An indicator of the 'age' of stratospheric air, *Geophys. Res. Lett.*, *18*, 763–766, 1991.

Stephens, G. L., D. L. Jackson, and I. Wittmeyer, Global observations of upper tropospheric water vapor derived from TOVS radiance data, *J. Clim.*, *9*, 305–326, 1996.

Takahashi, T., R. Wanninkhof, R. Feely, R. Weiss, D. C. N. Bates, J. Olafsson, C. Sabine, and S. Sutherland, Net sea-air CO_2 flux over the global oceans: An improved estimate based on the sea-air pCO_2 difference, in *Proceedings of the 2nd International Symposium on CO_2 in the Oceans*, National Institute of Environmental Studies, Tsukuba, Japan, 1999.

Tarantola, A., *Inverse Problem Theory: Methods for Data Fitting and Model Parameter Estimation*, Elsevier Sci., New York, 1987.

A. S. Denning, R. J. Engelen, K. R. Gurney, and G. L. Stephens, Department of Atmospheric Science, Colorado State University, Fort Collins, CO 80523, USA. (denning@atmos.colostate.edu; richard@atmos.colostate.edu; keving@atmos.colostate.edu; stephens@atmos.colostate.edu)

(Received August 15, 2000; revised March 9, 2001; accepted April 18, 2001.)